Journal of Food Measurement and Characterization (2022) 16:295–306
https://doi.org/10.1007/s11694-021-01162-8

ORIGINAL PAPER

Characterization of rheological properties of complex coacervates composed by whey protein isolate, chitosan and garlic essential oil

Loleny Tavares[1] · **Caciano Pelayo Zapata Noreña**[1]

Received: 17 July 2021 / Accepted: 5 September 2021 / Published online: 13 September 2021

Abstract

This work aims to study the effect of incorporation of garlic essential oil (GEO) with loading of 10% (GEO-10) and 20% (GEO-20) on the strength and stability of polyelectrolyte complex coacervate obtained by electrostatic interactions between chitosan (CH) and whey protein isolate (WPI) with positive and negative charges, respectively. Rheological studies were applied to investigate the viscosity and viscoelastic properties of complex coacervates. The viscoelastic properties were investigated by dynamic oscillatory tests and static tests (creep and recovery). The coacervates exhibited the shear-thinning behavior of non-Newtonian fluid, and the frequency sweep test revealed magnitude of elastic modulus (G′) higher than loss modulus (G″) at high frequency due to the formation of compact network structure with elastic dominant property (solid-like behavior). Arrhenius model was able to estimate the relationship between viscosity and temperature, and the high temperature caused molecular expansion and increase in intermolecular distances, leading to decrease on the viscosity. The energy of activation (E_a) was 25.24 and 20.74 kJ mol^{-1} for WPI/GEO-10/CH and WPI/GEO-20/CH, respectively. The highest E_a value for WPI/GEO-10/CH indicated the formation of more strength and structured network matrices for GEO protection. Creep and recovery data were well fitted by Burger model and exponential decay function, respectively, and obtaining R^2 higher than 0.98. The percentage recovery (*%R)* was 16.67% and 9.52% for WPI/GEO-10/CH and WPI/GEO-20/CH, respectively, indicating that WPI/GEO-10/CH had greater capacity for structural recovery and the most suitable to be applied in food product that industrially requires large stress, high temperature and long-time processes.

Keywords Garlic essential oil · Chitosan · Whey protein isolate · Complex coacervation

Introduction

Garlic is an herbaceous plant that belongs to the genus *Allium* and botanic family of *Liliaceae*; It originated from Central Asia and cultivated in the tropical and subtropical countries worldwide [1, 2]. One of the most important products derived from garlic is garlic essential oil, and its mainly bioactive compounds are sulfides derivatives, such as diallyl sulfide, diallyl disulfide, diallyl trisulfide and diallyl tetrasulfide [3, 4]. These compounds have diverse biological activities, including antiviral, antimutagenic, anticarcinogenic, antioxidant, antimicrobial, and effects on cholesterol levels [5]. However, essential oils contain unstable compounds capable of decomposition, volatilization and oxidation when subjected to harsh environmental conditions, namely high temperature, as well as the presence of oxygen and light [1, 6]. In addition, garlic essential oil have strong flavor and organoleptic characteristics that can alter the sensorial characteristic of product, affecting its application in some food products [1]. In this sense, different encapsulation methods have been employed in the protection of GEO against adverse environmental conditions. Complex coacervation is one of the encapsulation methods widely used in the protection of volatile compounds. This method consists of hydrogen bonding and electrostatic interactions between two oppositely charged colloidal species, which leads to the formation of two distinct and incompatible phases: a polymer-rich phase (coacervate) in equilibrium with a diluted solvent phase [2, 7]. The coacervate obtained from the complex coacervation process contains a high amount of solvent, which needs to be evaporated from the product and turned

✉ Caciano Pelayo Zapata Noreña
czapatan@ufrgs.br

[1] Institute of Food Science and Technology, Federal University of Rio Grande do Sul, Av. Bento Gonçalves, no. 9500, Porto Alegre, Rio Grande do Sul CEP 91501-970, Brazil

into powder using dehydration methods such as spray drying and freeze drying [8]. However, before drying process, the study of rheological properties is essential to understand the structural characteristics of the coacervate. Rheology is the science that studies the flow and deformation of fluids, and also describes how the materials react to applied stress or strain [9, 10]. Rheological analyses provide useful information about molecular interactions between polymers and consequent formation of network structure between them, allowing to assess details about specific molecular mechanism of encapsulation process that can be used to predict the final properties of microparticles [1, 11]. The determination of rheological properties of food products can provide useful scientific knowledge for food researchers during the phase of ingredient selection, proving important information for selecting and optimizing production techniques and implementation of suitable storage strategies [12]. The rheological measurements include the viscosity and viscoelastic properties of the samples. The viscoelastic fluid can be investigated using dynamic oscillatory tests and static tests (creep or recovery) [9, 10]. The ability to understand viscoelastic behavior of food products is crucial in the design and evaluation of its stability [13].

In the present study, chitosan (CH) and whey protein isolate (WPI) were used as wall materials in the encapsulation of GEO by complex coacervation method resulting from hydrogen bonding and electrostatic interactions between positively charged CH (pKa around 6.3) and WPI with a negative charge (isoelectric point about 5.2) [14, 15]. The conjugation between polysaccharide and protein has been demonstrated to be a promising way to enhance the emulsifying properties of polymers [16]. Yang et al. [17] reported concentration of 10% of GEO (on a total solid basis of wall material) to be optimum for encapsulation efficiency (80%) using polyethylene glycol as wall materials. However, different other studies have been reported oil loading of 20% (on a total solid basis of wall material) in the encapsulation of essential oils [18–21]. Tavares et al. [2], microencapsulated GEO with concentration of 10% (w/w) using two types of wall materials, namely soy protein isolate/chitosan and β-cyclodextrin, obtaining entrapment yield varying from 71.74 to 82.03%. However, studies about incorporation of GEO-10 (10%) and GEO-20 (20%) into the matrices of biopolymers and determination of rheological properties of coacervate composed by WPI/GEO/CH have not yet been carried out. Furthermore, the importance of this research is centered on evaluating the effect of incorporation of two different concentrations of GEO (10 and 20% on a total solid basis) on the network structure of WPI/CH coacervate by examining the rheological properties of the produced coacervates. Therefore, the objective of this study was to study the effect of (GEO) incorporation on the strength, stability and structure of polyelectrolyte complex coacervate phases ((WPI/GEO-10/CH and WPI/GEO-20/CH) according to rheological measurements of steady shear (viscosity), dynamic oscillatory (stress, frequency, temperature and time sweeps) and static (creep and recovery).

Materials and methods

Garlic essential oil (GEO), containing mainly 14.6% of allyl methyl sulfide, 26.3% of diallyl disulfide, 25.2% diallyl trisulfide, 5.5% of allyl methyl trisulfide, 12.9% of diallyl tetrasulfide, was acquired from Lazlo (Belo Horizonte, Brazil). Whey protein isolate and chitosan (CH) with deacetylation degree (DD) of 96% were generously provided by Arla Foods Ingredients (São Paulo, Brazil) and Primex (Siglufjordur, Iceland), respectively. Sodium acetate trihydrate and glacial acetic acid were purchased from CAQ – Casa da Química, and the hydrochloric acid (HCl) and sodium hydroxide (NaOH), both with analytical grade, were obtained from Sigma-Aldrich.

Encapsulation of garlic essential oil by complex coacervation

The dispersions of WPI and CH were prepared at 3% (w/w) in acetate buffer (100 mM) at pH 6 and pH 5.5, respectively, according to zeta potential analyses reported by Tavares and Noreña [22]. A magnetic stirrer was used to agitate both dispersions for 4 h and then allowed to rest for 24 h at −4 °C to ensure complete hydration. After that, GEO at concentration of 10% (GEO-10) and 20% (GEO-20) were slowly mixed with dispersion of WPI and then homogenized for 5 min at 6000 rpm in a high-speed homogenizer (Ultra-Turrax IKA, T18). Then, the dispersion of CH 3% (w/w) was gradually transferred to a flask with WPI/GEO-10 or WPI/GEO-10, resulting in dispersions of WPI/GEO-10/CH and WPI/GEO-20/CH, respectively. The dispersions were stirred with a magnetic stirrer (Fisaton, Model 752A) for 30 min. The result was the formation of two phases: a supernatant-rich phase (solvent) and a precipitated biopolymer-rich phase denominated by coacervate. The supernatants were discarded and each of precipitated coacervate was recovered for rheological characterization.

Rheological measurements

The rheological properties of WPI/GEO-10/CH and WPI/GEO-20/CH coacervates were carried out using strain-controlled rheometer (Thermo Scientific, HAAKE MARS 40/60, Karlsruhe, Germany) fitted with parallel plate geometries (35 mm in diameter) and gap of 1 mm. The viscosity and viscoelastic properties of the coacervate were determined according to the following studies.

Viscosity

The apparent viscosity was measured at 25 °C as a function of shear rate ($\dot{\gamma}$) that ranged from 0.1 to 100 s^{-1}. The effect of temperature on the apparent viscosity of the coacervates was evaluated using the Arrhenius model (Eq. 1) [23], at a constant shear rate of 0.1 s^{-1} and varying temperature from 20 to 80 °C.

$$\eta_a = A \exp\left(\frac{E_a}{RT}\right) \tag{1}$$

where η_a is the apparent viscosity (Pa s), A is a constant, T is the absolute temperature and R is the universal gas constant (8.3144621 J K^{-1} mol^{-1}), E_a is the energy of activation for flow curve (KJ mol^{-1}). In order to estimate the parameters, E_a and A for each coacervate at a specific temperature, Eq. (1) was transformed to (Eq. 2), and the values of E_a and A were determined as the slope and intercept, respectively, of a straight line of ln of η_a versus the reciprocal of absolute temperature (1/T):

$$\text{Ln}\,\eta_a = \text{Ln}\,A + \frac{E_a}{RT} \tag{2}$$

Viscoelastic properties

The viscoelastic properties of the coacervates were determined using the following two methods: dynamic oscillatory and static (creep or relaxation) tests.

Dynamic oscillatory test The dynamic oscillatory tests were investigated according with two procedures: large amplitude oscillatory shear tests (LAOS) and small amplitude oscillatory shear tests (SAOS). For LAOS tests, the stress sweep was evaluated to make certain that the amplitude oscillatory shear (SAOS) tests were made within the linear viscoelastic region (LVR). Stress sweep tests were investigated from 0.1 to 150 Pa at a fixed frequency of 1 Hz and 20 °C. Thereafter, a constant stress of 1 Pa (within the LVR) was selected for the following SAOS tests: (a) frequency sweep tests were performed from 0.01 to 100 Hz at 20 °C; (b) temperature sweep tests the samples were heated from 20 to 90 °C at a fixed frequency of 1 Hz; and (c) time sweep tests were performed during 1 h at fixed temperature of 20 °C and frequency of 1 Hz. The generated values of storage or elastic modulus (G′) and loss or viscous modulus (G″) were plotted as a function of stress, frequency, temperature, or time on a logarithmic scale. For the frequency sweep tests, the parameters of complex modulus (G^*) and complex viscosity (η^*) were evaluated according to Eqs. 3 and 4, respectively:

$$|G^*| = \sqrt{(G')^2 + (G'')^2} \tag{3}$$

$$\eta^* = \frac{G^*}{\omega} \tag{4}$$

The Carreau–Yasuda model (Eq. 5) was used to study the dependency of complex viscosity on angular frequency (ω in rad/s) [24].

$$\eta^*(\omega) = \eta_0^*\left[1 + \left(\frac{\eta_0^*}{\tau^*} \times \omega\right)^a\right]^{\frac{n-1}{a}} \tag{5}$$

where η_0^* is zero complex viscosity, n is the power-law index, a indicates the width of the transition region between Newtonian and non-Newtonian behavior and τ^* is the shear stress at the transition between Newtonian and non-Newtonian region, and the relaxation time (λ) was calculated according to Eq. 6 [25].

$$\lambda = \frac{\eta_0^*}{\tau^*} \tag{6}$$

Creep recovery tests In creep experiments, a small constant stress (1 Pa and within LVR) was applied over medium to long time periods, obtaining elastic or viscous deformation [26]. The results are expressed in terms of compliance J(t) against time, that expresses the relation between the generated deformation and applied stress [13].

The results are expressed in terms of compliance function against time are expressed according to Eq. 7 [15]:

$$J_t = \frac{\gamma(t)}{\tau_0} \tag{7}$$

where τ_0 is the constant stress applied (Pa) and $\gamma_{(t)}$ is the resulting dependent strain time during the test. Creep compliance was defined as J_c over the creep time (from 0 to 180 s) by applying a constant stress (τ_0) of 1 Pa (within the LVR), and the recovery compliance was defined as J_R for the recovery time (from 180 to 360 s) after removal of stress (constant stress equal to 0). The Burger model was used to describe the creep (J_C) compliance (Eq. 8) (representing the Maxwell and Kelvin–Voigt models placed in series), and recovery (J_R) compliance was described by an exponential decay function (Eq. 9) [27, 28].

$$J_c = \frac{1}{G_0} + \frac{1}{G_1} \times \left[1 - \exp\left(\frac{-tG_1}{\eta_1}\right) + \frac{t}{\eta_0}\right] \tag{8}$$

where G_0 and η_0 represent the mechanical Maxwell model of instantaneous shear modulus and residual viscosity (dashpot contribution), respectively, and G_1 and η_1 represent the mechanical Kelvin–Voigt model of shear modulus

(representing the retarded elastic region) and internal viscosity (dashpot contribution), respectively.

$$J_R = J_\infty + J_{1R} \exp\left(-Bt^C\right) \quad (9)$$

where J_∞ and J_{1R} represent the recovery compliance of the Maxwell dashpot and Kelvin–Voigt element, respectively, and B and C are parameters that define the recovery speed of the system.

The samples' capacity to recover was calculated according to Eq. 10:

$$\%R = \frac{J_{max} - J_\infty}{J_{max}} \quad (10)$$

where $\%R$ is the total percentage recovery, and J_{max} and J_∞ represent the maximum compliance verified and the recovery compliance of the Maxwell dashpot, respectively.

Statistical analysis

Statistical analysis was performed using SAS software (v. 9.3). Generated data were exposed to Analysis of Variance (ANOVA), and mean comparison of different treatments was evaluated using Tukey's test ($p < 0.05$). The Burger model parameters and the parameters of exponential decay function were evaluated according to the Levenberg–Marquardt algorithm in the MATLAB® curve-fitting toolbox.

Results and discussion

Viscosity

Viscosity of the fluid can be described as a system's resistance provided by the adjacent layers to one another during the flow of the fluid [29]. The viscosity of the WPI/GEO-10/CH and WPI/GEO-20/CH coacervates are shown in Fig. 1. The coacervates exhibited typical pseudoplastic fluid with shear-thinning behavior of non-Newtonian behavior, where the apparent viscosity decreases with increased shear rate [9, 10]. Shear thinning occurs primarily as a result of network strength caused by underlying electrostatic forces between biopolymers, leading to a structural change in the coacervates [30]. According to the results, two distinct regions can be identified: (a) from 0.1 to 40 s^{-1} where the apparent viscosity (η) decrease as the shear rate increased, and (b) from 40 to 100 s^{-1} identified as Newtonian region where the apparent viscosity was constant with changing shear rates. From the shear rate higher than 40 s^{-1}, the disruption of entanglements polymers chain results in rearrangement in the conformation of the polysaccharides molecules and entanglement density; therefore, a horizontal Newtonian plateau is obtained without reduction in the viscosity since

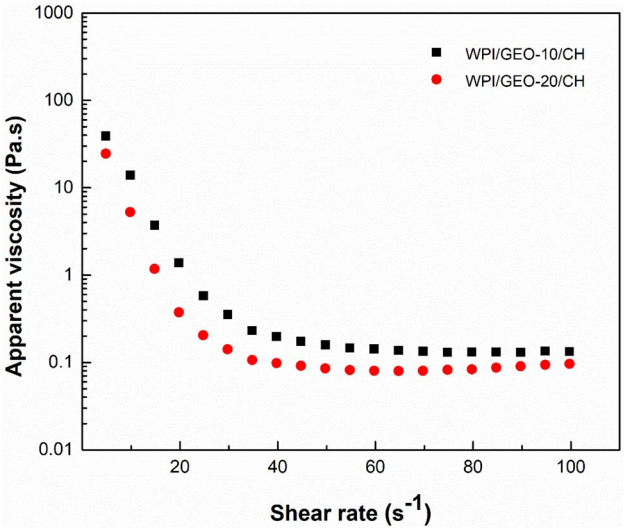

Fig. 1 Apparent viscosity as a function of shear rate between 0.1 to 100 s^{-1} for WPI/GEO-10/CH (filled square) and WPI/GEO-20/CH (filled circle) coacervates

all the chains are disentangled [31–33]. According to You et al. [34], the network structure of coacervate at greater shear rates is not stable, resulting in the breaking of physical bonds and structure disintegration. This phenomenon is associated with polymeric polysaccharide solutions with a high macromolecular weight [35]. The highest GEO concentration interfered in the chain entanglement and the network structure of the coacervate by reducing the resistance of the polymer chains mobility. According to Bordón et al. [36], presence of oil droplets disturbs the flow of the fluid, increasing the energy dissipation. It's possible to conclude that the disentanglement of coacervate macromolecular chains was less accentuated for WPI/GEO-10/CH, obtaining a flow curve behavior with higher viscosity at higher shear rate.

Effect of temperature on apparent viscosity

The effect of temperature on the apparent viscosity of the coacervates was examined from the temperature of 20 to 90 °C at a fixed shear rate ($\dot{\gamma}$) of 0.1 s^{-1}, corresponding to the $\dot{\gamma}$ value where the network structure of the coacervate is less affected by the applied stress (high viscosity) (Fig. 2).

The viscosity of both coacervates decreased with increased temperature until 70 °C, and then is verified an increase in the viscosity until the end of the test. The decrease in viscosity can be attributed to the disruption of the chain entanglement and increases in the intermolecular spaces caused the thermal expansion, leading to the reduction of intermolecular forces and consequently decrease in the viscosity of the sample [31, 37, 38].

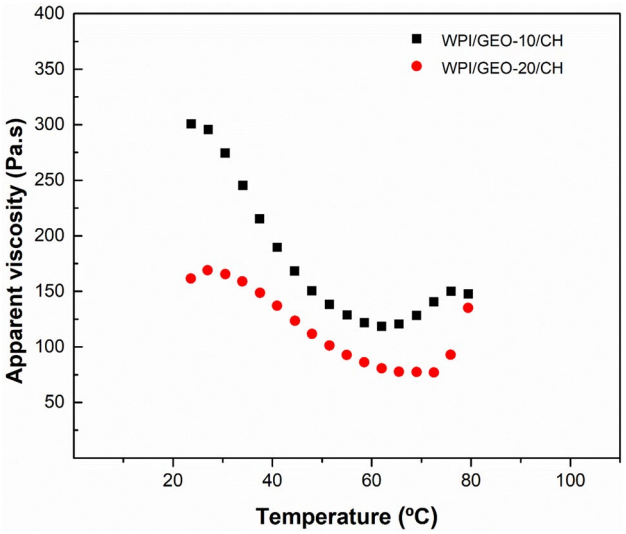

Fig. 2 Apparent viscosity versus temperature from 20 to 80 °C for WPI/GEO-10/CH (filled square) and WPI/GEO-20/CH (filled circle) coacervates

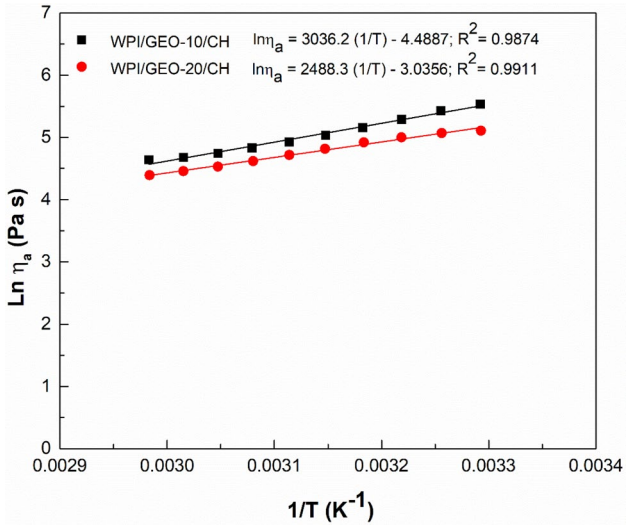

Fig. 3 Arrhenius plots of apparent viscosity (η_a) versus the inverse of absolute temperature (T) for WPI/GEO-10/CH (filled square) and WPI/GEO-20/CH (filled circle) coacervates

According to Zhang et al. [39], higher temperatures cause molecular expansion and an increase in intermolecular distances, leading to decrease on the apparent viscosity. The results suggesting that WPI/GEO-20/CH coacervate has more flexible molecular conformation as compared with the WPI/GEO-10/CH, and the temperature rise caused higher disruption of its chain entanglement and network structure.

The emulsification process had an important role during the encapsulation process by complex coacervation method, since it is used as starting point of this method. Therefore, since the emulsion formation involves shearing, it is necessary to comprehend concepts such as activation energy, which is defined as barrier, induced by the resistance of the surrounding building units, to overcome to allow molecules to move during the viscosity measurements [31]. The effect of temperature (30–60 °C) on the apparent viscosity of the coacervates at a fixed shear rate (0.1 s^{-1}) is shown in Fig. 3, using the Arrhenius model (Eq. 1) to estimate the relationship of apparent viscosity and temperature.

The temperature ranges of 30 to 60 °C corresponds to the region where the Arrhenius model was able to estimate the relationship of viscosity and temperature, obtaining values of R^2 of 0.9874 and 0.9911 for WPI/GEO-10/CH and WPI/GEO-20/CH, respectively (Fig. 3). From the adjusted data, the regression analysis of ln η_a versus 1/T (Fig. 3) allowed to estimate the magnitudes of E_a from the slope of linear regression analysis multiplied by the universal gas constant (8.3144621 J K^{-1} mol^{-1}) (Eq. 2).

The values of E_a were 25.24 and 20.74 kJ mol^{-1}, whereas the values of constant A were 0.01 and 0.05 for WPI/GEO-10/CH and WPI/GEO-20/CH, respectively. The WPI/GEO-10/CH coacervate showed higher value of E_a than WPI/GEO-20/CH, indicating that the viscosity of WPI/GEO-10/CH coacervate was more sensitive to temperature change. The high value of E_a also indicate formation of a dense and structured matrix around the active compounds capable to protect them against thermal stress [31, 40]. Chaharlang and Samavati [41] reported that the high value of E_a is related to the decrease in the chain flexibility during the flow process. Therefore, the GEO compounds present in the WPI/GEO-10/CH coacervate are more protected against thermal stress than GEO compounds of WPI/GEO-20/CH coacervate. This result also suggest that molecular chain entanglement was stronger than disentanglement, resulting in more energy in molecular motion [39]. This result indicates that WPI/GEO-10/CH complex is more suitable to be applied in food products that require high-temperature heating, and also products susceptible to high temperature changes during the processing, handling and storage.

Dynamic oscillatory test

Stress sweep

The dependence of storage modulus (G′) and loss modulus (G″) on the stress for are represented in Fig. 4. The storage modulus G′ represents the magnitude of the energy that is stored in the material or recoverable per cycle of deformation, whereas G″ is a measure of the energy which is lost as viscous dissipation per cycle of deformation, and the magnitudes of both parameters are influenced by stress, frequency, temperature, and time [9]. Stress sweeps are used to estimate the linear viscoelasticity region (LVR) in which a system may withstand maximal deformation

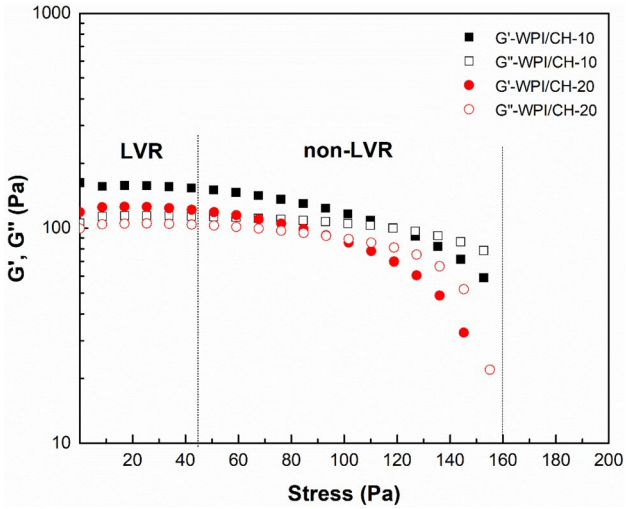

Fig. 4 Stress sweep test for WPI/GEO-10/CH (square) and WPI/GEO-20/CH (circle) coacervates. Filled and empty symbols represent storage modulus (G′) and loss modulus (G″), respectively

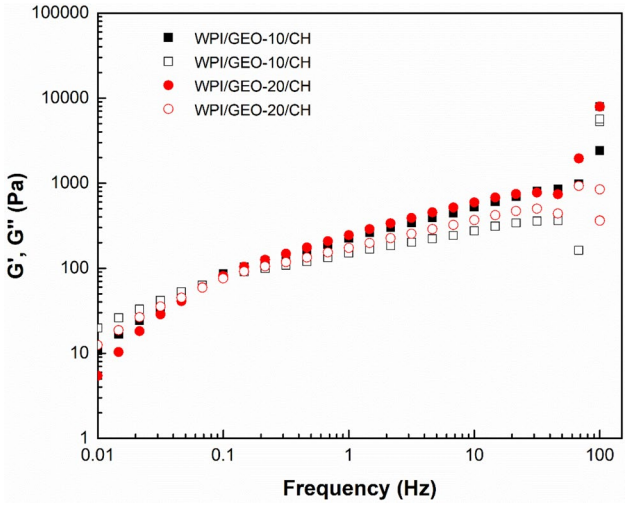

Fig. 5 Frequency sweep test for WPI/GEO-10/CH (square) and WPI/GEO-20/CH (circle) coacervates determined at constant temperature of 20 °C and fixed stress of 1 Pa. Filled and empty symbols represent storage modulus (G′) and loss modulus (G″), respectively

(critical strain) without causing permanent structural damage [2]. According to Fig. 4, with increasing stress, two different regions were obtained: an LVR where G′ and G″ were almost constant, and non-linear viscoelastic region (non-LVR) in which G′ and G″ started to decrease until the end of the test. The WPI/GEO-10/CH coacervate showed higher values of G′ and G″ than WPI/GEO-20/CH coacervates, indicating that the increase in the concentration of GEO from 10 to 20% resulted in a decrease in the magnitudes of both G′ and G″ moduli. This result indicates that the incorporation of GEO into the network matrices of the coacervate promote alteration in their structural strength, leading to the formation of coacervate with less compact and rigidity structure. Similar results were reported by Tavares and Noreña [15] in the encapsulation of ginger essential oil by complex coacervation using WPI/gum Arabic (GA) and CH/GA as complex wall materials.

The results of stress sweep test, corresponding to the LAOS experiment, indicated that the increase of stress causes damage on the network structure of both complexes. This finding can be useful to predict the coacervate behavior during handing, processing and storage conditions, and can be used to understand how complex materials behave under high conditions of stress, which is fundamental for optimization and design purposes since a wide variety of industrial processes involve large stress. This finding can be useful to predict the coacervate behavior during handing, processing and storage conditions, and can be used to understand how complex materials behave under high conditions of stress, which is fundamental for optimization and design purposes since a wide variety of industrial processes involve large stress [2].

Therefore, the stress of 1 Pa, within the linear viscoelastic region, was used in the SAOS tests (frequency, temperature and time sweeps), avoiding any modification of the molecular structure caused by stress, since in this region the network structure of coacervate was not damaged by the stress imposed during the stress sweep measurements.

Frequency sweep test

The frequency sweep measurements were employed to study the effect of GEO concentration on the network structure of coacervates (Fig. 5).

The magnitude of G′ and G″ increased with increased values of frequency for both coacervates. The coacervates showed magnitudes of G″ higher than the G′ at frequency below 10 Hz, and then occur the crossover point (G″ = G′) and the magnitudes of G′ became higher than G″.

According to Zhang et al. [39], at low frequencies, the molecular chains had enough time to disentangle and reorder, whereas at high frequencies the molecular chains had less time to disentangle, and the entanglement points contributed to a temporary cross-linking junction zone.

This result indicates greater firmness of the coacervates and formation of a compact network and stronger network structure. According to Yang et al. [42], material with compact structure has more elastic behavior since the movement of the molecular chains are more difficult. At low frequency, the coacervate behaved similarly to a weak gel with liquid-like behavior (G″ > G′), while at higher frequencies (2.5 Hz)

the coacervate behaved similarly to a strong gel with solid-like behavior (G″ < G′). According to Steffe [10], the crossover lines between G′ and G″ at centered frequency range indicates concentrated solutions with solid-like behavior at higher frequencies. In this sense, it is possible to conclude that the high values of frequency coacervate induced the formation of stronger network structure with solid-like behavior. Samples with magnitude of G′ higher than G″ indicate the formation of stronger network structure [43]. Yuan et al. [44] investigated the rheological behavior of complex coacervate composed by soy protein isolate/algal oil/chitosan, and they reported the formation of highly linked network structures with values of G′ higher than G″.

The WPI/GEO-10/CH and WPI/GEO-20/CH coacervates revealed similar viscoelasticity properties, and the effect of incorporation of 10 and 20% of GEO on the biopolymers matrices is not clear using the frequency sweep test. Therefore, the analyses of the parameter's complex modulus (G*) and complex viscosity were evaluated to investigate possible differences between the structure of the WPI/GEO-10/CH and WPI/GEO-10/CH coacervates (Fig. 6).

The complex viscosity (η*) decreased linearly with increase in frequency, indicating that the coacervates had

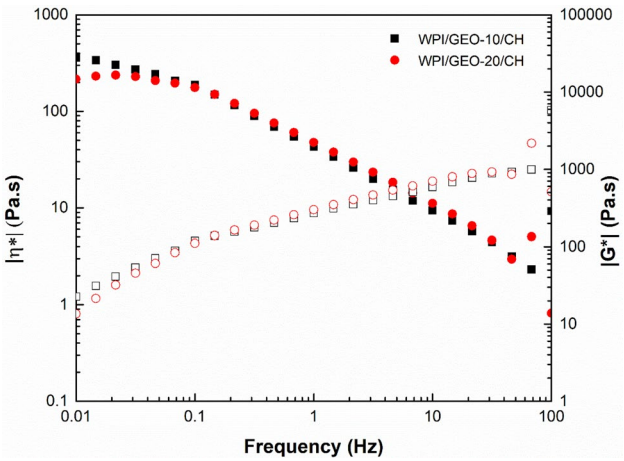

Fig. 6 Complex viscosity (η*) (filled) and complex modulus (G*) (empty) as a function of frequency (Hz) for WPI/GEO-10/CH (square) and WPI/GEO-20/CH (circle) coacervates

non-Newtonian behavior of shear-thinning fluid. The high frequency causes permanent molecular misalignment or disentanglement of long chain polymers, and a decrease in complex viscosity [45]. The shear-thinning behavior for higher frequency is in accordance with the results of apparent viscosity reported in Fig. 1. The magnitudes of G* increased with frequency, indicating that the high frequency induced the formation of a compact, strong and stable network structure, preventing the molecular chains movement in both coacervates. The strengthening of the gel-network is mainly due to the enhancement of attractive forces of van der Waals interactions and hydrogen bonding between hydrocolloid particles, resulting in the formation of gel structure with higher degree of cross-linking and/or entanglement [46]. According to Zare et al. [47], at low frequencies, the polymer chains have enough time for relaxation, obtaining lower values of G*, and at high frequencies (short-range deformation) the polymer chains cannot relax and hardly deform increase the values of G*. The WPI/GEO-10/CH and WPI/GEO-20/CH coacervates showed curves with similar behavior, which are in concordance with the results of frequency sweep test represented in Fig. 5. In this sense, the Carreau–Yasuda model was used to fit the experimental complex viscosity data in order to verify possible differences between the structure of the WPI/GEO-10/CH and WPI/GEO-10/CH coacervates. This model can be applied to complex viscosity data to study the shear thinning behavior and the Newtonian and non-Newtonian regions of the samples. The values of Carreau–Yasuda model parameters are presented in Table 1.

The Carreau-Yasuda model was suitable to fit the experimental complex viscosity data, obtaining values of R^2 higher than 0.99 for both coacervates. The WPI/GEO-10/CH showed higher values of η_0^* and τ^* than WPI/GEO-20/CH coacervate, confirming its stronger and compact network structure. The high values of relaxation time (λ) obtained for WPI/GEO-10/CH indicate stronger interfacial interaction between polymer chains, and also lower mobility of polymer chain [25]. Moreover, WPI/GEO-20/CH showed lower values of parameters n, indicating more shear thinning behavior. The parameter a, which represents the width of the transition region between Newtonian and non-Newtonian

Table 1 The estimated values of Carreau–Yasuda model parameters for the WPI/GEO-10/CH and WPI/GEO-20/CH coacervates

Complex	Carreau model parameters					
	η_0^*(Pa s)	τ^*	a	n	λ	R^2
WPI/GEO-10/CH	448.10 ± 29.13^{a}**	144.90 ± 7.82^{a}	0.80 ± 0.04^{a}	0.25 ± 0.02^{b}	3.09	0.9984
WPI/GEO-20/CH	229.90 ± 12.18^{b}	113.30 ± 7.02^{b}	2.33 ± 0.17^{b}	0.38 ± 0.02^{a}	2.03	0.9974

**Different letters (a and b) in the same column indicate values that are significantly different ($p < 0.05$) based on Tukey's multiple comparison test. η_0^* is the zero complex viscosity; n is the power-law index; a indicates the width of the transition region between Newtonian and non-Newtonian behavior; τ^* is the shear stress at the transition between Newtonian and non-Newtonian region; λ is the relaxation time

regions, was higher for WPI/GEO-20/CH due to its weaker network structure and high width of the transition between the Newtonian to non-Newtonian regions.

Temperature sweep test

The temperature sweep curves with variation G′ and G″ moduli upon heating from 20 to 90 °C at a fixed frequency (1 Hz) and stress (1 Pa) are shown in Fig. 7.

The coacervate showed a storage modulus (G′) higher than the loss modulus (G″), in the entire range of investigated temperatures. There was no crossover point for G′ and G″, which indicates that the coacervate structure was predominantly elastic and remains in the solid-like behavior during the whole range of investigated temperatures. The values of G″ and G′ decrease with increased temperature until 70 °C and 75 °C for WPI/GEO-10/CH and WPI/GEO-20/CH, respectively, and then was verified abruptly increased of both moduli for both coacervates. The initial decrease in G′ and G″ can be related to the increase in fluidity with increasing temperature, which can be attributed to the energy dissipation movement of the molecules and decrease in intermolecular interactions [48]. The initial decrease in G′ and G″ can be related to the increase in fluidity with increasing temperature, which can be attributed to the energy dissipation movement of the molecules and decrease in intermolecular interactions [48].

The temperature in the region between 70 and 75 °C indicate the point where the whey proteins present in coacervate start to denature and the elastic modulus starts to invert the decreasing trend, and the elastic module fits the standard heat-set whey protein gelation behavior [49]. Similar result was reported by Yang et al. [42], indicating that the changes in G′ and G″ with temperature result from protein unfolding due to the denaturation of the protein myosin present in surimi. For the temperature above 70 °C and 75 °C for WPI/GEO-10/CH and WPI/GEO-20/CH, respectively, the results suggest reorganization of the network structure of the coacervate, causing the strengthening of the structures mainly due to formation of three-dimensional network structure with a strong gel-like behavior. The G′ was always greater than G″ throughout the temperature range covered. This result indicates the formation of a strong gel-like network structures with increased temperature [43]. In addition, the coacervates can show a solid-like behavior even at high temperatures and their structures get stronger for the temperature above 65 and 80 °C for WPI/GEO-10/CH and WPI/GEO-20/CH, respectively. The magnitudes of G′ and G″ were higher for WPI/GEO-10/CH than WPI/GEO-20/CH complex at two temperature range: 20 to 40 °C, and 70 to 90 °C and WPI/GEO-20/CH. This result confirms a stronger network structure for WPI/GEO-10/CH coacervate, which was less affected by increasing temperature. Samples with strong network structure and improved mechanical strength, hardness, gumminess, and stiffness are desirable in the context of industrial application [43].

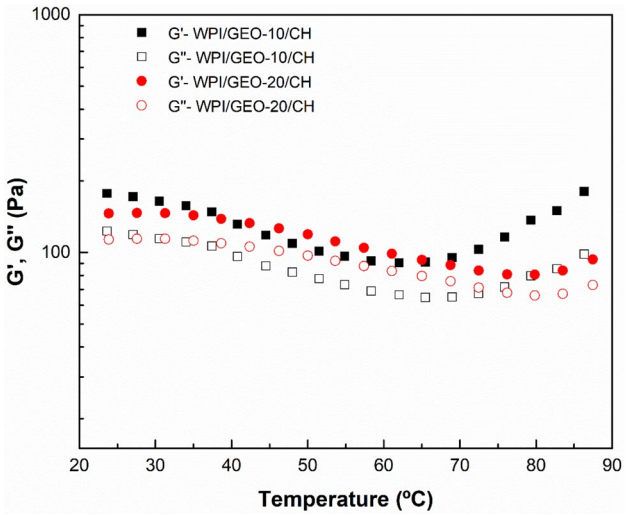

Fig. 7 Temperature sweep test for WPI/GEO-10/CH (filled square) and WPI/GEO-20/CH (filled circle) coacervates determined at constant frequency of 1 Hz and fixed stress of 1 Pa. Filled and empty symbols represent storage modulus (G′) and loss modulus (G″), respectively

Time sweep test

Oscillatory time sweeps are important in the rheological measurements of dispersions, and polymers that may undergo macro-or micro-structural rearrangement with time [50]. This concept is applied for the complex coacervation method, where is required time to rearrangement and formation of the entanglement network structure. The temperature sweep curves with changes in G′ and G″ as a function of time for 1 h at fixed frequency of 1 Hz and temperature of 20 °C for WPI/GEO-10/CH and WPI/GEO-20/CH coacervates are illustrated in Fig. 8.

For both coacervates, the values of G′ were higher than G′ for the entire aging time, indicating that elastic component predominated over the viscous component G″. The G′ and G″ values were not remarkably changed during 30 min. After that, the magnitudes of G′ and G″ increased sharply, representing a reinforcement of the polymer networks structure of the complex of WPI/CH coacervate. The values of G′ were higher than G″, indicating that the elastic behavior of the structure of coacervate predominated over its viscous behavior during over tested time. The G′ and G″ values for WPI/GEO-10/CH was higher than obtained for WPI/GEO-20/CH throughout the entire tested time. This result indicates that WPI/GEO-20/CH exhibited weaker elastic character as compared with WPI/GEO-10/CH coacervate, and the incorporation of high concentration of GEO in the polymeric

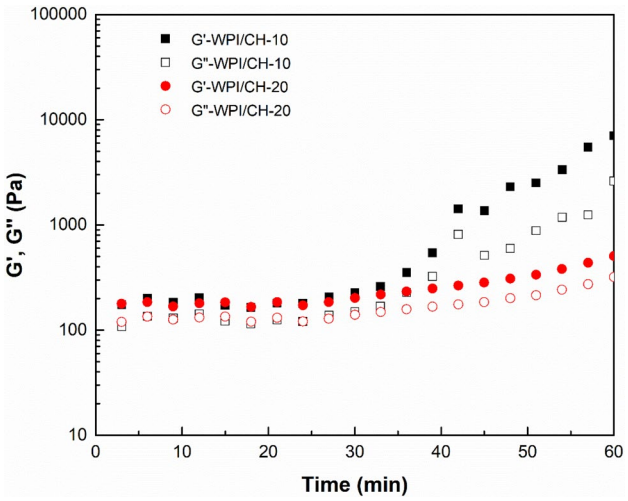

Fig. 8 Time sweep test for WPI/GEO-10/CH (square) and WPI/GEO-20/CH (circle) coacervates determined at constant frequency of 1 Hz, fixed stress of 1 Pa and temperature of 20 °C. Filled and empty symbols represent storage modulus (G′) and loss modulus (G″), respectively

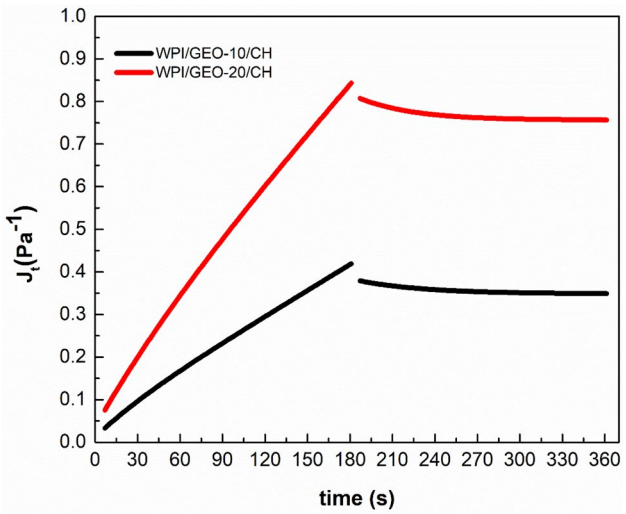

Fig. 9 Compliance (J_t) versus time in creep phase (from 0 to 180 s) and recovery phase (from 180 to 360 s) for WPI/GEO-10/CH (black) and WPI/GEO-20/CH (red) coacervates

matrices of the wall materials resulted in the formation of lesser compact network structure. Coacervate with strong, compact and stable network structure are desirable during the production of microparticles, since strong, stable and compact network structure of colloidal material suffer less changes when subjected to high shear stress during industrial application [2].

The viscoelastic properties of the WPI/GEO-10/CH and WPI/GEO-20/CH coacervates determined by the SAOS test suggest that the presence of high concentration of GEO decreases the rigidity and entanglement of the network structure of the coacervates. The internal network structure of both coacervates is greatly affected by the high values of temperature, frequency and time employed at end of the tests, causing some structural alteration and molecular rearrangement (Figs. 2, 5, 7 and 8).

Creep and recovery

Creep and recovery tests were performed to determine the values of compliance ($J(t)$), which represent the deformation of samples caused by the application of shear stress [13]. The creep and recovery tests have been employed to study the internal structure of a material, and its structural changes associated with the introduction of some alteration on the initial composition [51]. In the creep-recovery test, samples with stronger, compact and stable structures have lower J_t values, while samples with weaker network structure have higher J_t values [52]. Creep-recovery tests were performed to determine the influence of GEO incorporation on the matrices of biopolymers and the results of J_t for the complex coacervates with and without GEO the creep and recovery phases are showing in Fig. 9.

For the creep phase, constant stress of 1 Pa was applied to samples for 180 s, and the increase of creep compliance (J_c) corresponds to the deformation of the coacervate structure caused by the applied stress within the LVR. The WPI/GEO-10/CH showed lower magnitudes of J_c, indicating the formation of a stronger structure. The higher values of J_c obtained for WPI/GEO-20/CH indicates coacervate with weaker network structure. These results confirmed that the incorporation of GEO on the matrices of biopolymers caused a reduction on the rigidity of coacervate, leading to the formation of a less compact structure, confirming the results obtained for viscosity (Fig. 1) and temperature and time sweep tests represented in the Figs. 7 and 8, respectively. The formation of a stronger network structure results in lower creep compliance values [15]. Tavares and Noreña [22] reported similar results for the encapsulation of ginger essential oil by complex coacervation using complex of whey protein isolate/gum Arabic and gum Arabic/chitosan as wall materials, suggesting alterations in the structural characteristic of the coacervates.

Burger model was applied in order to study the creep phase behavior, and this model result by the association of the Maxwell and Kelvin–Voigt models in series, and the determination of its four parameters (G_0, G_1, η_0 and η_1) allow to compare the internal structure of different systems [51]. The Burger model parameters are presented in Table 2.

In both cases, the coefficients of determination (R^2) were higher than 0.98, indicating that the creep phase was well fitted by the Burger model. The G_0 provides results of magnitude intensity of the elastic strength on the molecular

Table 2 The fitting parameters of Burger model for WPI/GEO-10/CH and WPI/GEO-20/CH coacervates

Complex	Burger model parameters				
	G_0 (Pa)	G_1 (Pa)	η_0 (Pa s)	η_1 (Pa s)	R^2
WPI/GEO-10/CH	85.65 ± 3.51^{a}**	23.62 ± 0.97^{a}	20.97 ± 0.65^{b}	844.20 ± 34.81^{a}	0.9894
WPI/GEO-20/CH	28.52 ± 1.45^{b}	7.44 ± 0.45^{b}	35.71 ± 2.18^{a}	463.10 ± 28.25^{b}	0.9998

**Different letters in the same column indicate values that are significantly different ($p < 0.05$) based on Tukey's multiple comparison test. G_0 is the instantaneous shear modulus of the Maxwell unit; G_1 is the shear modulus of Kelvin–Voigt; η_0 is the residual viscosity (dashpot contribution) of the Maxwell element; η_1 is the internal viscosity (dashpot contribution) of Kelvin–Voigt unit

bonds present in the interfacial network structure [52]. In this sense, the highest value of G_0 obtaining for WPI/CH reflect its greater elasticity with a stronger and compact network structure formed by entanglement of the biopolymer's chains. In contrast, the WPI/GEO-20/CH coacervate with high GEO concentration showed the lowest G_0, which was mainly due to its characteristic of the weaker gel with less compact network structure. The parameter G_1 reflects the magnitude of the retarded elastic deformation and the resistance to deformation caused by the three-dimensional network structure [53]. The highest G_1 value indicated the formation of a more complex network structure rich in zone junctions, whereas the lowest G_1 value indicated the formation of a simpler network structure with lower junction's zones [53, 54]. The highest G_1 value obtaining WPI/GEO-20/CH confirms that the GEO interfered in the structure of WPI/CH complex. The viscosity parameters η_0 (associated with the Maxwell dashpot) and η_1 (associated with Kelvin–Voigt dashpot) also decreased when the amount of GEO incorporated in the network structure of WPI/CH increases, causing the gel flow more easily due to the decrease of the resistance to the flow.

In any food system, the decrease in values of Burger model parameters is mainly due to its weakened network structure, which allows for decreases in shear moduli and viscosity [27]. Samples with a compact, stale and robust network structure have greater viscoelastic properties and less deformations in their internal structure during the creep–recovery measurements [15].

The results of obtained for the four Burger model parameters indicate that there is a relationship between the viscoelastic properties determined by the oscillatory dynamic test and the static test (creep phase). According to Parot and Duperray [55], for a linear viscoelastic material, there is a relationship between the complex modulus, the creep function and the relaxation modulus.

The recovery phenomenon was monitored in the end of the creep period during 180 s, where the constant stress applied was zero. Parameters estimated of J_∞, J_{1R}, C, B, J_{max}, and final percentage recovery of samples ($\%R$) are shown in Table 3. Both coacervates showed R^2 higher than 0.99, confirming that the exponential decay function (Eq. 4) fitted well the recovery phase data. The WPI/GEO-20/CH showed significantly ($p < 0.05$) higher values of J_∞ and J_{max} than WPI/GEO-10/CH, indicating that the high GEO concentration induce the formation of a weaker and softer network structure, whereas WPI/GEO-10/CH showed the lowest values of J_∞ and J_{max} due to its more rigidity, stable, compact internal network structure. These results are in accordance with the obtained in the creep phase and dynamic oscillatory frequency sweep test. The WPI/GEO-20/CH coacervate showed superior values of parameter C (related to the curvature shape) and inferior values for B parameter (showing less phase magnitude in compliance decay). The WPI/GEO-10/CH showed higher percentage recovery ($\%R$) values due to its higher capacity for structural recovery, suggesting stronger interaction between the polymer chain as compared with WPI/GEO-20/CH [15]. The high value of $\%R$ for WPI/GEO-20/CH indicates the formation of structure with more viscous behavior. The total recovery shape and degree of material deformation are affected by the length of the test, the amount of stress applied, and the temperature of the sample [56].

Table 3 The fitting parameters of empirical model for WPI/GEO-10/CH and WPI/GEO-20/CH coacervates

Complex	J_∞ (Pa^{-1})	J_{max} (Pa^{-1})	J_{1R} (Pa^{-1})	$B \times 10^{-3}$	C	$\%R$ (%)	R^2
WPI/GEO-10/CH	0.35 ± 0.03^{b}**	0.42 ± 0.01^{b}	0.83 ± 0.05^{b}	6.20 ± 0.44^{a}	1.20 ± 0.06^{b}	16.67	0.9843
WPI/GEO-20/CH	0.76 ± 0.04^{a}	0.84 ± 0.01^{a}	1.67 ± 0.10^{a}	2.90 ± 0.24^{b}	1.37 ± 0.11^{a}	9.52	0.9902

**Different letters in the same column indicate values that are significantly different ($p < 0.05$) based on Tukey's multiple comparison test. J_{max} is the maximum compliance; J_∞ is the compliance of the Maxwell dashpot; J_{1R} is the Kelvin–Voigt element; $\%R$ is the final percentage recovery; B and C are the constant parameters of systems

Conclusion

The viscosity and viscoelastic properties determined by oscillatory measurements (stress, frequency, temperature and time sweeps) and static test (creep and recovery) revealed suitable to obtain information about internal network structure, stability and strength of produced complex coacervates. This study demonstrated that the incorporation of garlic essential oil in the biopolymers matrices with loading of 20% (on a total solid basis of wall material) result in coacervate with less compact and rigidity structure as compared with loading of 10%. The coacervate with GEO of 10% (WPI/GEO-10/CH) showed higher viscosity than coacervate with GEO of 20% (WPI/GEO-20/CH). The WPI/GEO-10/CH coacervate showed higher value of energy of activation (25.24 kJ mol^{-1}) than that obtained for WPI/GEO-10/CH (20.74 kJ mol^{-1}), indicating that WPI/GEO-10/CH had more compact and structured matrix to protect GEO compounds. The stress, time and temperature sweep tests indicated that WPI/GEO-10/CH tended to form the more stable viscoelastic solutions compared to WPI/GEO-20/CH. Therefore, WPI/GEO-10/CH coacervate revealed most suitable for industrial applications that involve large stress, long time and high temperature. The potential application of complex coacervate as active ingredients in the elaboration of food products should be evaluated in future studies. In addition, further research should be conducted to study the textural properties, particle size, morphology, glass transition temperature, thermal properties, and sensory evaluation in order to assess the relationship with rheological analyses.

Acknowledgements The authors acknowledge the financial support provided from FAPERGS and CNPq. We thank the Primex (Siglufjordur, Iceland) and Arla Foods Ingredients for donating chitosan and whey proteins isolates, respectively. Loleny Tavares also thanks CAPES/CNPq-Programa Estudantes-Convênio de Pós-Graduação (PEC-PG) for scholarship funding.

Funding Funding was provided by Conselho Nacional de Desenvolvimento Científico e Tecnológico (Grant No. 306489/2018-0), Fundação de Amparo à Pesquisa do Estado do Rio Grande do Sul (Grant No. 17/2551-0000915-0), Coordenação de Aperfeiçoamento de Pessoal de Nível Superior.

References

1. L. Tavares, L. Santos, C.P. Zapata Noreña, Trends Food Sci. Technol. **114**, 232 (2021)
2. L. Tavares, L. Santos, C.P.Z. Noreña, Powder Technol. **390**, 103 (2021)
3. C.T. Ho, J. Li, M.C. Kuo, in *Flavor Chemistry of Ethnic Foods*. ed. by F. Shahidi, C.T. Ho (Springer, Boston, 1999), pp. 55–76
4. S.G. Santhosha, P. Jamuna, S.N. Prabhavathi, Food Biosci. **3**, 59 (2013)
5. M. Corzo-Martínez, N. Corzo, M. Villamiel, Trends Food Sci. Technol. **18**, 609 (2007)
6. N. Ozdemir, A. Bayrak, T. Tat, F. Altay, M. Kiralan, A. Kurt, J. Food Meas. Charact. **15**, 1865–1876 (2021)
7. S. Rojas-Moreno, F. Cárdenas-Bailón, G. Osorio-Revilla, T. Gallardo-Velázquez, J. Proal-Nájera, J. Food Meas. Charact. **12**, 650–660 (2018)
8. M. Lengyel, N. Kállai-Szabó, V. Antal, A.J. Laki, I. Antal, Sci. Pharm. **87**, 20 (2019)
9. M.A. Rao, in *Rheology of Fluid, Semisolid, and Solid Foods: Principles and Applications*. ed. by M.A. Rao (Springer, Boston, 2014), pp. 27–61
10. J.F. Steffe, *Rheological Methods in Food Process Engineering* (Freeman Press, New York, 1996)
11. C. Wandrey, A. Bartkowiak, S.E. Harding, in *Encapsulation Technologies for Active Food Ingredients and Food Processing*. ed. by N.J. Zuidam, V. Nedovic (Springer, New York, 2010), pp. 31–100
12. H. Dogan, J.L. Kokini, *Batters and Breadings in Food Processing* (AACC International Press, Washington, 2011), pp. 263–299
13. A. Ibarz, G.V. Barbosa-Cánovas, *Unit Operations in Food Engineering* (CRC Press, Boca Raton, 2002)
14. L. Tavares, H.L.B. Barros, J.C.P. Vaghetti, C.P.Z. Noreña, Food Bioprocess Technol. **12**, 2093 (2019)
15. L. Tavares, C.P.Z. Noreña, Food Hydrocoll. **89**, 360 (2019)
16. L.H. Wang, X. Sun, G.Q. Huang, J.X. Xiao, J. Food Meas. Charact. **12**, 2718–2724 (2018)
17. F.L. Yang, X.-G. Li, F. Zhu, C.L. Lei, J. Agric. Food Chem. **57**, 10156 (2009)
18. C. Valcourt, P. Saulnier, A. Umerska, M.P. Zanelli, A. Montagu, E. Rossines, M.L. Joly-Guillou, Int. J. Pharm. **498**, 23 (2016)
19. N. Parris, P.H. Cooke, K.B. Hicks, Encapsulation of essential oils in zein nanospherical particles. J Agric Food Chem. **53**, 4788 (2005)
20. Y.I. Chang, J. Scire, B. Jacobs, *Flavor Encapsulation* (American Chemical Society, Washington, 1988), pp. 87–102
21. L.P. Fernandes, I.C.C. Turatti, N.P. Lopes, J.C. Ferreira, R.C. Candido, W.P. Oliveira, Dry. Technol. **26**, 1534 (2008)
22. L. Tavares, C.P.Z. Noreña, Food Bioprocess Technol. **13**, 1405 (2020)
23. J. Steffe, Introduction to rheology. Rheol. Methods Food Process. Eng. **2**, 1 (1996)
24. K. Yasuda, Massachusetts Institute of Technology, 1979.
25. Y. Zare, S.P. Park, K.Y. Rhee, Results Phys. **13**, 102245 (2019)
26. V.S. Kulkarni, C. Shaw, Rheological studies, in *Essential Chemistry for Formulators of Semisolid and Liquid Dosages*. ed. by V.S. Kulkarni, C. Shaw (Academic Press, Boston, 2016), pp. 145–182
27. S. Karaman, M.T. Yilmaz, H. Cankurt, A. Kayacier, O. Sagdic, Food Res. Int. **48**, 507 (2012)
28. M.T. Yilmaz, S. Karaman, M. Dogan, H. Yetim, A. Kayacier, J. Food Eng. **108**, 327 (2012)
29. A.K. Sharma, A.K. Tiwari, A.R. Dixit, Sust. Energ. Rev. **53**, 779 (2016)
30. Y. Liu, H.H. Winter, S.L. Perry, Adv. Colloid Interface Sci. **239**, 46–60 (2017)
31. W. Rosas-Flores, E.G. Ramos-Ramírez, J.A. Salazar-Montoya, Carbohydr. Polym. **98**, 1011 (2013)
32. H. Gong, M. Liu, J. Chen, F. Han, C. Gao, B. Zhang, Carbohydr. Polym. **88**, 1015 (2012)
33. Y. Wei, Y. Guo, R. Li, A. Ma, H. Zhang, Food Hydrocoll. **110**, 106198 (2021)
34. G. You, X.L. Liu, M.M. Zhao, Food Hydrocoll. **74**, 255–266 (2018)
35. M. Fathi, Z. Emam-Djomeh, A. Sadeghi-Varkani, Int. J. Biol. Macromol. **120**, 1265–1274 (2018)
36. M.G. Bordón, A.J. Paredes, N.M. Camacho, M.C. Penci, A. González, S.D. Palma, P.D. Ribotta, M.L. Martinez, Powder Technol. **391**, 479–493 (2021)
37. Q. Xiao, Q. Tong, L.T. Lim, Carbohydr. Polym. **87**, 1689 (2012)

38. H. Toğrul, N. Arslan, Mathematical model for prediction of apparent viscosity of molasses. J. Food Eng. **62**, 281 (2004)
39. L. Zhang, Z. Liu, X. Han, Y. Sun, X. Wang, Int. J. Biol. Macromol. **134**, 807–814 (2019)
40. A.L. Muñoz-Celaya, M. Ortiz-García, E.J. Vernon-Carter, J. Jauregui-Rincón, E. Galindo, L. Serrano-Carreón, Carbohydr. Polym. **88**, 1141 (2012)
41. M. Chaharlang, V. Samavati, Int. J. Biol. Macromol. **79**, 56 (2015)
42. Y. Yang, X. Liu, Y. Xue, C. Xue, Y. Zhao, Food Hydrocoll. **98**, 105260 (2020)
43. L. Tavares, E.E. EsparzaFlores, R.C. Rodrigues, P.F. Hertz, C.P.Z. Noreña, Food Hydrocoll. **106**, 105876 (2020)
44. Y. Yuan, Z.Y. Kong, Y.E. Sun, Q.Z. Zeng, X.Q. Yang, LWT **75**, 171–179 (2017)
45. L. Wang, H.M. Liu, C.Y. Zhu, A.J. Xie, B.J. Ma, P.Z. Zhang, Carbohydr. Polym. **209**, 230 (2019)
46. A. Rafe, S.M.A. Razavi, Food Hydrocoll. **62**, 58–65 (2017)
47. Y. Zare, K.Y. Rhee, Compos. B **156**, 100 (2019)
48. M.A. Hesarinejad, A. Koocheki, S.M.A. Razavi, Food Hydrocoll. **35**, 583 (2014)
49. C.M.R. Rocha, H.K.S. Souza, N.F. Magalhães, C.T. Andrade, M.P. Gonçalves, Carbohydr. Polym. **110**, 345 (2014)
50. M.V. Chandra, B.A. Shamasundar, Food Hydrocoll. **48**, 47 (2015)
51. M. Dolz, M.J. Hernández, J. Delegido, Food Hydrocoll. **22**, 421 (2008)
52. J. Huang, S. Zeng, S. Xiong, Q. Huang, Food Hydrocoll. **61**, 48 (2016)
53. M.G. de Alcântara, N. de FreitasOrtega, C.J.F. Souza, E.E. Garcia-Rojas, Food Struct. **24**, 100137 (2020)
54. Y.Y. Chang, D. Li, L.J. Wang, C.H. Bi, B. Adhikari, Carbohydr. Polym. **108**, 183 (2014)
55. J.M. Parot, B. Duperray, Mech. Mater. **40**, 575 (2008)
56. M. Cabuk, M. Yavuz, H.I. Unal, Colloids Surf. A **510**, 231–238 (2016)